Modelling of the failure behaviour of windscreens and component tests

Authors:

D.-Z. Sun, Fraunhofer Institute for Mechanics of Materials
F. Andrieux, Fraunhofer Institute for Mechanics of Materials
A. Ockewitz, Fraunhofer Institute for Mechanics of Materials

H. Klamser, Dr. Ing. h.c. F. Porsche AG
J. Hogenmüller, Dr. Ing. h.c. F. Porsche AG

Correspondence:

Wöhlerstrasse 11, 79108 Freiburg, Germany
Tel: 0049 761 5142 193
Fax: 0049 761 5142 401
dong-zhi.sun@iwm.fraunhofer.de

Weissach, Germany

Keywords:
Laminated safety glass, finite elements, crash simulation, fracture

ABSTRACT

Windscreens from laminated safety glass (glass/PVB interlayer/glass) are widely used in automotive structures and have an important contribution to the stiffness of the vehicle. The stiffness of the laminated safety glass is dominantly given by the two layers of glass while the PVB interlayer serves to fix glass splinters to avoid serious injuries of the passengers in a collision. A finite element model for modelling the failure behaviour of laminated glass windscreens is presented. A special element structure with three layers (shell/volume/shell) has been used to model the laminated glass windscreen. A fracture criterion for brittle fracture based on the maximum principal stress ($\sigma_I \geq \sigma_c$) was applied to model the fracture behaviour of glass. The PVB interlayer was modelled with both a linear elastic and a hyperelastic material law without damage. The critical fracture stress of glass was determined by fitting the failure force measured from static bending tests on laminated glass windscreens. The transferability of the fracture criterion and the corresponding parameter was checked by simulating two different loading cases of the component tests.

INTRODUCTION

Automotive windscreens today are usually made from laminated safety glass. Laminated safety glass is constructed by placing an adhesive polyvinyl butyral (PVB) interlayer between two glass panes. The purpose of the interlayer is to prevent the glass panes from shattering on impact, thus greatly reducing the possibility of injury caused by pieces of flying glass. As the pieces of broken glass adhere to the tear proof PVB interlayer after fracture, there is no complete collapse of the windscreen and it still contributes to the stiffness of the vehicle. The modelling of the failure behaviour of laminated glass windscreens is important for the assessment of occupant safety and a precise prediction of the load-bearing capacity of the whole vehicle in crash simulation.

It is well known that under crash loading glass shows a linear elastic behaviour until fracture, while the PVB interlayer displays a viscoelastic behaviour. Some experimental and numerical works about crash simulation of laminated glass windscreens have been done [1, 2]. Nevertheless, there are still no simple methods available for the determination of relevant material data, especially with regard to fracture behaviour. Moreover, verified fracture criteria and efficient models for the simulation of the damage behaviour of the windscreens are lacking.

The main objective of this work therefore is to determine material parameters describing the fracture of laminated glass windscreens by simulation and comparison with relevant experiments and to supply a verified finite element model for crash simulation of laminated safety glass.

Experimental Investigations

To establish a basis for the validation of the finite element model static bending tests on laminated glass windscreens have been performed with a variation of loading conditions. For the tests the windscreens were put on four spherical supports with a radius of 75 mm and loaded by a rigid sphere with a radius of 150 mm from the inner to the outer side (load case 1) and from the outer to the inner side (load case 2). The loading velocity was 0.08 mm/s. Fig. 1 shows a photograph of the test setup for load case 1. The test setup for the two different load cases is further illustrated in Fig. 6 and Fig. 7.

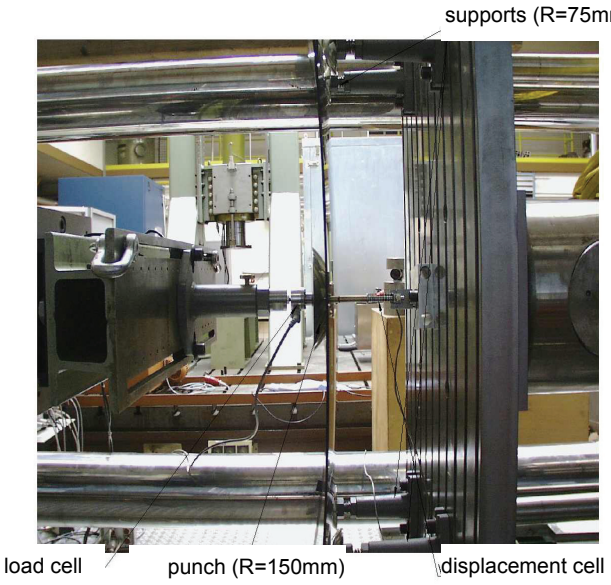

Fig. 1: Test setup for load case 1 (from the inner to the outer side)

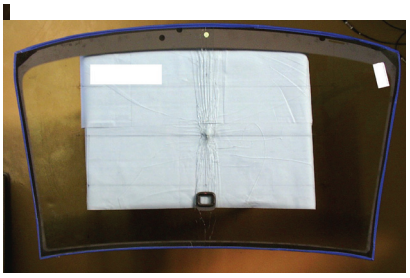

Fig. 2: Fracture pattern of windscreen (load case 1)

Three windscreens were loaded from the inner to the outer side. The measured load vs. displacement curves are depicted in Fig. 3. After crack initiation the glass panes of all three windscreens immediately fail reducing forces to zero. The forces resp. displacements at fracture differ considerably for the three windscreens. Fig. 2 and Fig. 13 left (detail) show the typical fracture pattern for this load case. Fracture spreads laterally across the whole windscreen and does not stay localized.

The load vs. displacement curves (Fig. 4) as well as the fracture patterns (Fig. 14 left) of the four windscreens loaded from the outer to the inner side are different from those of load case 1. The cracks in the glass panes arise circularly and radially around the contact patch of the punch and do not propagate to the pane rims. The forming of the cracks corresponds to the first drop in load in the load vs. displacement curves. As the cracks do not grow further the measured loads increase again and do not fall to zero as in load case 1.

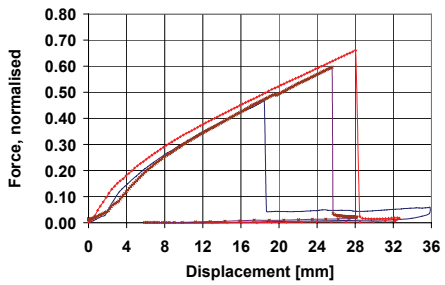

Fig. 3: Measured load vs. displacement curves (load case 1)

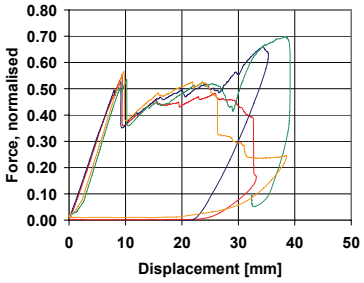

Fig. 4: Measured load vs. displacement curves (load case 2)

FE modelling and material models

The calculations were performed with the crash codes LS-DYNA [4] and ABAQUS/Explicit [3]. In the finite element simulations, three elements with coincident nodes at their boundaries are used to model the layered structure of the laminated safety glass: two shell elements for the outside and inside glass layers and a solid element for the PVB interlayer. To position the shell elements corresponding to the thickness of the glass layers the shell midsurfaces are offset from their reference surface (containing the element nodes) by half the glass layer/shell thickness. Fig. 5 shows the layer structure of the finite element model. Complete FE-models of the windscreens for the two load cases of the bending tests are shown in Fig. 6 and
Fig. 7.

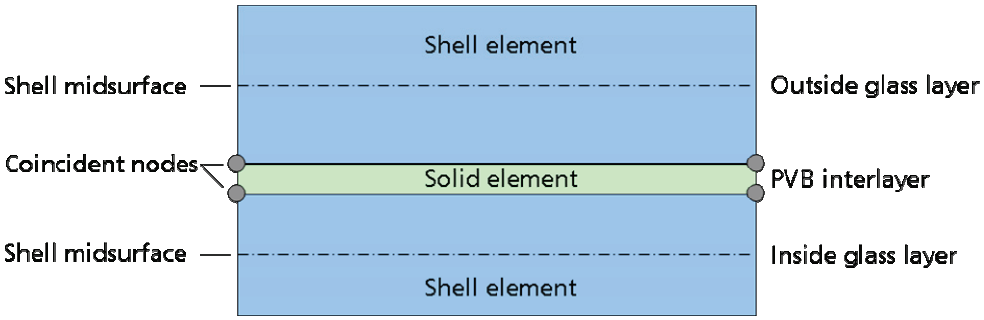

Fig. 5: Layer structure of the finite element model for laminated safety glass

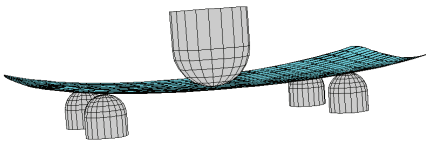

Fig. 6: FE-model for load case 1 (from the inner to the outer side)

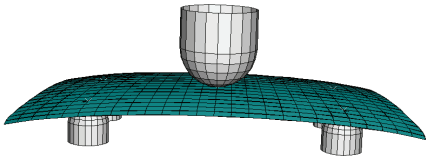

Fig. 7: FE-model for load case 2 (from the outer to the inner side)

For comparison, the PVB interlayer was modelled with both a linear elastic and a hyperelastic material law.

Linear elastic model
The PVB foil was first modelled using a linear elastic model with values of 9 MPa and 0.49 for the Young's modulus and the Poisson's ratio, respectively, taken from literature [1].
Hyperelastic model
At low strain rate and room temperature the PVB foil shows a rubberlike behaviour which can be modelled using a hyperelastic model. In this section, we restrict our attention to the Mooney-Rivlin model [5,6]. For an isotropic hyperelastic material the strain energy potential U depends on the strain invariants of the deformation

$$U = U(\bar{I}_1, \bar{I}_2, J)$$

where J=det **F** is the relative volume, **F** is the deformation gradient, $\bar{I}_1$ and $\bar{I}_2$ are the first and second invariant of the left Cauchy-Green strain tensor $\bar{\mathbf{B}} = J^{-2/3}\,\mathbf{B} = J^{-2/3}\,\mathbf{F}\mathbf{F}^{\mathbf{T}}$.

The Cauchy stress σ is obtained by

$$\sigma = \frac{2}{J}\mathrm{Dev}\left[\left(\frac{\partial U}{\partial \bar{I}_1} + \bar{I}_1 \frac{\partial U}{\partial \bar{I}_2}\right)\bar{\mathbf{B}} - \frac{\partial U}{\partial \bar{I}_2}\bar{\mathbf{B}}\bar{\mathbf{B}}\right] + \frac{\partial U}{\partial J}\mathbf{1}.$$

The form of the Mooney-Rivlin strain energy potential is

$$U = C_{10}\left(\bar{I}_1 - 3\right) + C_{01}\left(\bar{I}_2 - 3\right) + \frac{1}{D_1}(J-1)^2.$$

C_{10}, C_{01} and D_1 are material parameters, the initial bulk modulus K_0 and shear modulus G_0 can be expressed as

$G_0 = 2\,(C_{10} + C_{01})$, $K_0 = 2/D_1$.

In the incompressible case the deformation gradient for a uniaxial loading is given by

$$\mathbf{F} = \begin{bmatrix} \lambda & 0 & 0 \\ 0 & \lambda^{-1/2} & 0 \\ 0 & 0 & \lambda^{-1/2} \end{bmatrix}$$

where λ is the stretch. The technical strain ε_{tech} and stress σ_{tech} are obtained by

$$\varepsilon_{tech} = \lambda - 1 \qquad \sigma_{tech} = 2(1-\lambda^{-3})(\lambda C_{10} + C_{01}).$$

The true stress vs. strain curves from a uniaxial tensile test obtained with the linear elastic model (E=9 MPa, ν=0.49) and the Mooney-Rivlin model are compared with experimental data for PVB in Fig. 8. According to the work of Du Bois et al. [2] the hyperelastic parameter set C_{10}=1.45, C_{01}=0.06 und D_1=0.013 was chosen. In order to investigate the parameter influence, the parameter set C_{10}=0, C_{01}=1.51 and D_1=0.013 was also used. Both parameter sets correspond to an initial Young's modulus of 9 MPa.

It has to be noted that for strains ε < 0.15 all material models yield coincident results, only for higher strains the results differ increasingly.

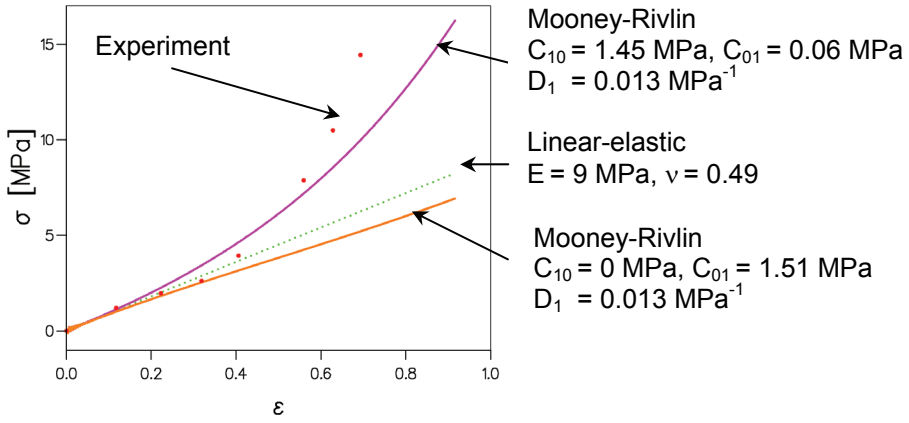

Fig. 8: Stress vs. strain curves for a tensile test, comparison between elastic, hyperelastic models and experimental data

Simulations of the bending tests with both a linear elastic and a hyperelastic material for the foil were performed using ABAQUS/Explicit. It was found that for load case 1 it does not have any effect to use an elastic or hyperelastic model as long as the same initial E-modulus is used. In this case an abrupt rupture occurs. As long as the glass does not fail, it constrains the PVB deformation and a linear

elastic model is suitable. In order to fit the experimental results a Young's modulus of 3 MPa was used. For load case 2 not only the initial E-modulus has an effect on the global behaviour but also the type of model (elastic or hyperelastic). For this load case failure occurs gradually. When the glass fails the PVB is able to undergo large deformation. Moreover, its behaviour subsequently dominates. Since experimental data are not available for the hyperelastic parameters, the PVB interlayer was modelled with the linear elastic material model. It was found that using the same Young's modulus of 3 MPa for the PVB interlayer as in the ABAQUS simulations the forces calculated by LS-DYNA are lower. Therefore, the Young's modulus was set to 9 MPa for the LS-DYNA calculations.

Glass shows linear elastic behaviour and then fails by brittle fracture, when a certain critical stress is exceeded. A material model "Brittle Cracking" for the simulation of such materials is available in ABAQUS/Explicit. This material model includes a stepwise reduction of tensile stresses after crack initiation. As glass fails abruptly and crack propagation is unstable, this stepwise reduction of stresses can be omitted from the calculations regarding an application for glass. Therefore a simplified version of the "Brittle Cracking" model where an element is immediately eliminated when the critical fracture stress is exceeded has been implemented as a user routine VUMAT for ABAQUS/Explicit.

For the simulations with LS-DYNA the elasto plastic material model MAT_123 which includes the fracture criterion $\varepsilon_I \geq \varepsilon_c$ has been equivalently used for the glass. Linear elastic material behaviour was modelled by artificially increasing the yield stress and the critical fracture stress for the glass was converted to a critical fracture strain. A survey of the material models used for the glass is given in the following table.

ABAQUS (Brittle Cracking)	ABAQUS (User-Routine)	LS-DYNA (MAT_123)
- linear elastic - onset of fracture: $\sigma_I \geq \sigma_c$ - crack extension perpendicular to σ_I - stepwise reduction of tensile stresses	- linear elastic - element elimination when $\sigma_I \geq \sigma_c$ by option "DELETE"	- elasto plastic - element elimination when $\varepsilon_I \geq \varepsilon_c$
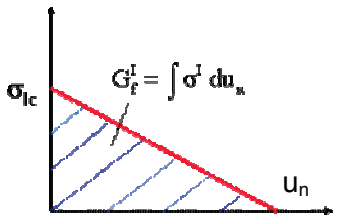		Application: - linear elastic behaviour by artificially increased yield stress - conversion: $\varepsilon_c = \sigma_c / E_{glass}$

Component simulation

The bending tests on the laminated safety windscreens were firstly simulated with a finite element model with an element length of 20 mm. The critical fracture stress was determined by fitting the calculated failure load to the tests for load case 1 (loading from the inner to the outer side of the windscreen). Fig. 9 shows the measured load vs. displacement curves in comparison with the calculated curve. The critical fracture stress was determined as 65 MPa.

To check the transferability of the fracture criterion for different element sizes the bending tests were additionally simulated with a finer and a coarser mesh with element lengths of 10 resp. 50 mm. In the first instance the fracture stress determined for the mesh with an element length of 20 mm was used for these simulations. The calculated load vs. displacement curves are compared in Fig. 10 with the measured ones. Fig. 10 shows that the calculated failure load depends considerably on the element size of the finite element model. In order to achieve comparable results between meshes of different element sizes the critical fracture stress has to be adjusted. This adjustment has again been done for load case 1. The dependence of fracture stress on element length L_e is depicted in Fig. 12.

Because of the high computational cost of the simulations the calculations for the adjustment of the fracture stresses were at first performed by imposing a loading rate five to ten times faster than the final one. For the model with an element length of 10 mm a dependence of fracture stress on computational speed was observed because of stress oscillations in the faster calculations. The fracture stress to be used for L_e = 10 mm therefore has to be higher than depicted in Fig. 12.

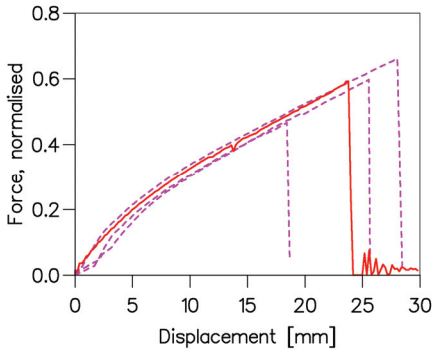

Fig. 9: Load vs. displacement curve (load case 1), L_e=20mm (experiment in dashed lines)

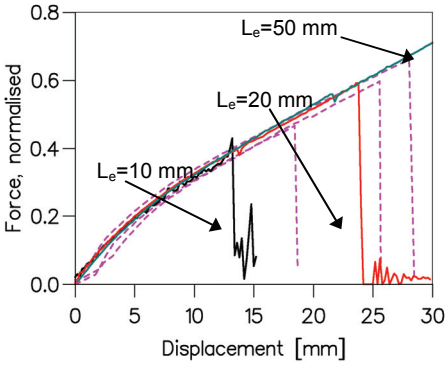

Fig. 10: Load vs. displacement curve (load case 1), L_e=10, 20 and 50 mm (experiment in dashed lines)

For validation of the finite element model the bending tests for load case 2 were simulated using the material data and fracture stresses that were determined for load case 1. Fig. 11 shows the measured load vs. displacement curves in comparison with the calculated curve for an element length of 20 mm. The calculated displacement at failure agrees well with the measured one, but the calculated load level after crack initiation is considerably higher than in the tests. Also crack initiation occurs too late in the simulation. Possible reasons for these deviations might be differences in properties, bonding conditions, residual stresses between the two glass panes that have not been taken into account in the simulations.

The simulations for the models with element lengths of 10 resp. 50 mm with the corresponding fracture stresses determined for load case 1 yield coincident results.

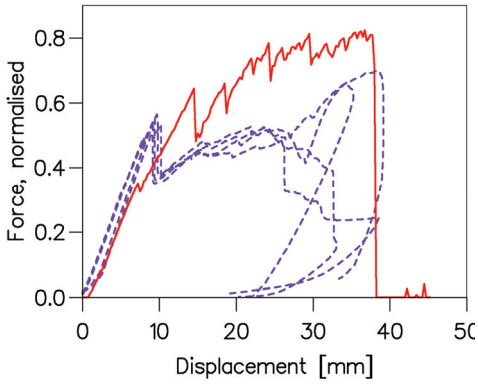

Fig. 11: Load vs. displacement curve (load case 2), L_e=20mm (experiment in dashed lines)

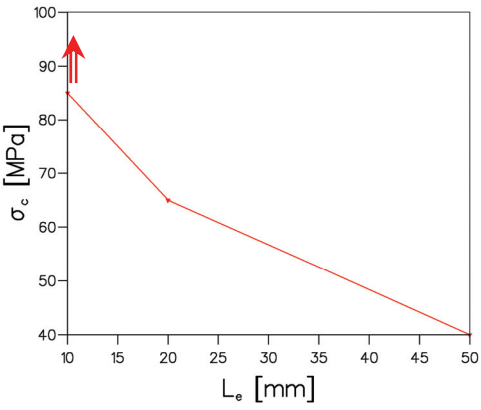

Fig. 12: Fracture stress vs. element length

The calculated fracture patterns together with photographs taken after the tests are shown in Fig. 13 for load case 1 and in Fig. 14 for load case 2. The calculated fracture patterns agree well with the experimental findings. For load case 1 cracking crosses the whole windscreen and is limited to a

narrow band. For load case 2 cracks form radially and circularly around the punch. The numerical results shown here were produced with ABAQUS/Explicit and the element size of the mesh is 10 mm. As for the coarser meshes due to the size of the eliminated elements the damaged zones are bigger than in reality, finer meshes – even with element lengths below 10 mm – are more appropriate for a realistic reproduction of the fracture behaviour of the glass panes.

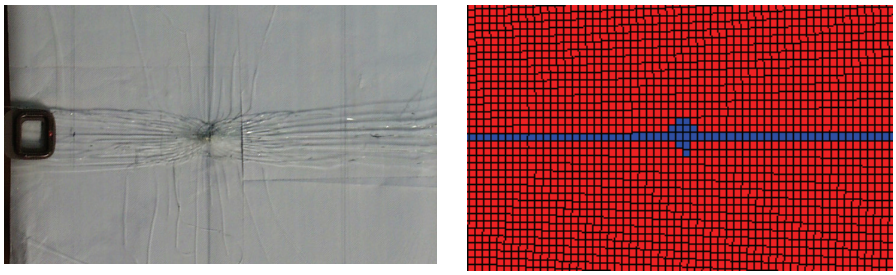

Fig. 13: Fracture pattern for load case 1, experiment (left) and simulation with L_e=10mm (right)

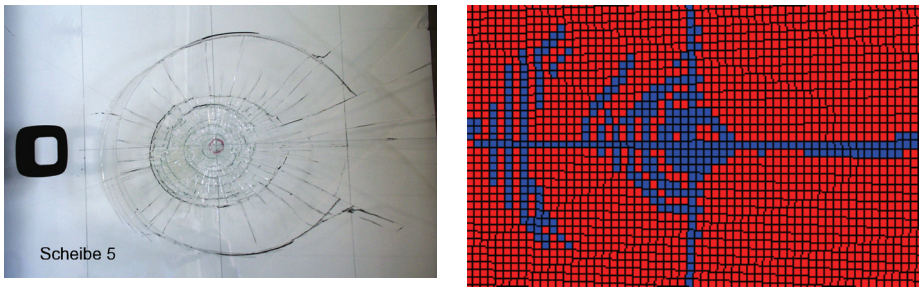

Fig. 14: Fracture pattern for load case 2, experiment (left) and simulation with L_e=10mm (right)

Fig. 15 shows the evolution of damage and the distribution of the maximum principal stress at four punch displacements for load case 2 and again an element size of 10 mm. These results were produced with LS-DYNA. Before the onset of fracture (punch displacement 14 mm) the maximum of the first principal stress spreads circularly around the punch. Also initial damage (punch displacements 22 mm and 36 mm) is calculated in a nearly circular shape. With increasing damage the maximum principal stress increases in the vicinity of the damaged zone due to element elimination and the next elements fail in this region. This leads to the cross-shaped fracture pattern that is observed at the end of the simulation.

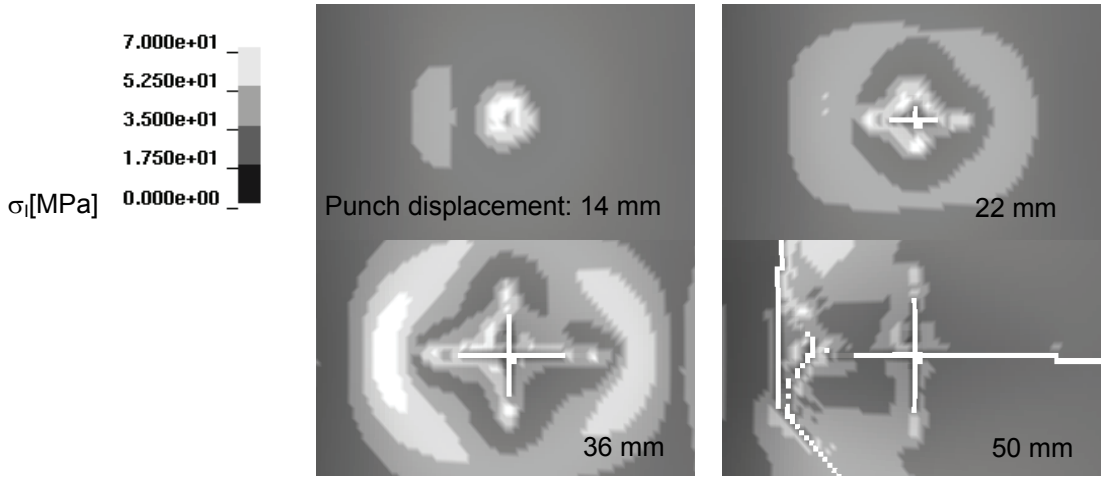

Fig. 15: Evolution of damage and distribution of maximum principal stress, L_e=10mm

Summary and Conclusions

It was found that the element structure with three element layers in combination with the suggested damage criterion for glass is applicable for the crash simulation of the laminated safety windscreen. The calculations with the linear elastic and the hyperelastic model for the PVB interlayer show different global responses in the loading phase after rupture of glass. The calculated failure load depends considerably on the element size of the finite element model. Therefore, a relationship between the critical fracture stress and element edge length has been derived for vehicle simulations by simulating a component test with different element sizes. The calculations were performed with the crash codes LS-DYNA and ABAQUS/Explicit. Some differences were identified between the results obtained from the two codes.

References

1. H. Kordisch, I. Varfolomeev, M. Sester, H. Werner, Numerical simulation of the failure behaviour of wind-shields, 32nd ISATA, Vienna, June 1999, 299-306.

2. P.A. Du Bois, S. Kolling, W. Fassnacht, Modelling of safety glazing materials for crash simulation, Computional Material Science, 28/3-4, 2003, 675-683.

3. ABAQUS User's Manual; Version 6.4, ABAQUS, Inc. (2003).

4. LS-DYNA Keyword User´s Manual, Version 970/Rev 5424, Livermore Software Technology Corporation, Sepember 2004.

5. M. Mooney, A theory of large elastic deformation, J. Appl. Physics, 1940, 11: 582-592.

6. R.S. Rivlin, Large elastic deformations of isotropic materials, Proc. Roy. Soc. London, 1948, 241: 379-397.